Analytical MSMAR versus Numerical HYDRUS-1D: Comparative Performance Analysis in the Estimation of Soil Water Components

Farid Faridani, Ph.D.[1]; Seyed Mohammadreza Naghedifar, Ph.D.[2]; Faezeh Karimian, Ph.D.[3]; Boris Basile, Ph.D.[4]; Ali Naghi Ziaei, Ph.D.[5]; Alireza Faridhosseini, Ph.D.[6]; Mauro Fiorentino, Ph.D.[7]; Fabio Madonna, Ph.D.[8]; and Rosa Lasaponara, Ph.D.[9]

Abstract: In this study, the performance of the modified soil moisture analytical relationship (MSMAR) in concurrent estimation of deep soil moisture (DSM), evapotranspiration (ET), and deep percolation (DP) derived from surface soil moisture (SSM) variations on a sprinkler-irrigated Triticale farm in northeast Iran was investigated. Soil moisture content across the growing season was monitored using time-domain reflectometry (TDR) sensors at seven depths down to 3 m, deployed at five locations on the farm. For model evaluation, HYDRUS-1D served as the benchmark, utilizing initial soil hydraulic parameters derived from RETC and ROSETTA software based on soil texture measurements. As a resource-efficient model, MSMAR underwent two calibration schemes employing MATLAB's genetic algorithm. The first scheme aimed to minimize the MSMAR's DSM errors with the TDR measurements, resulting in MSMAR's consistent DP and ET estimates comparable to those of HYDRUS-1D. Notably, the performance of the MSMAR's DSM estimates is equal or superior than those of HYDRUS-1D depending on the soil simulation depth. The second calibration scheme aimed to minimize the errors between the MSMAR's outputs with those of HYDRUS-1D (i.e., SM, ET and DP) demonstrating MSMAR adaptability relying on minimal information about soil texture, climate, and surface soil moisture variations. Detailed analysis via percentage root mean square error and R^2 values across depths highlighted MSMAR's superior performance within the 50–100 cm soil depth. HYDRUS-1D's consideration of root water uptake led to sharp declines in DSM and DP at the Triticale root depth (100 cm), contrasting MSMAR's gradual decline continuing to 200 cm. As a promising tool, MSMAR can be implemented in diverse environmental applications, notably in resource-scarce regions. **DOI: 10.1061/JIDEDH.IRENG-10454.**

Author keywords: Deep percolation; Evapotranspiration; Root zone; Surface soil moisture; Sprinkler irrigation.

[1]Postdoctoral Researcher, Dept. of Agricultural Sciences, Univ. of Naples Federico II, via Università 100, Portici, NA 80055, Italy (corresponding author). ORCID: https://orcid.org/0000-0002-1541-2695. Email: farid.faridanibardaskan@unina.it

[2]Assistant Professor, Dept. of Water Science and Engineering, Ferdowsi Univ. of Mashhad, Mashhad 9177948974, Iran. Email: s.m.rezanaghedifar@mail.um.ac.ir

[3]Postdoctoral Researcher, Dept. of Physics "E.R. Caianiello", Univ. of Salerno, Fisciano, SA 84084, Italy. Email: fkarimiansarakhs@unisa.it

[4]Associate Professor, Dept. of Agricultural Sciences, Univ. of Naples Federico II, via Università 100, Portici, NA 80055, Italy. ORCID: https://orcid.org/0000-0002-4207-576X. Email: boris.basile@unina.it

[5]Associate Professor, Dept. of Water Science and Engineering, Ferdowsi Univ. of Mashhad, Mashhad 9177948974, Iran. Email: an-ziaei@um.ac.ir

[6]Associate Professor, Dept. of Water Science and Engineering, Ferdowsi Univ. of Mashhad, Mashhad 9177948974, Iran. Email: farid-h@um.ac.ir

[7]Full Professor, Dept. of European and Mediterranean Cultures, Environment, and Cultural Heritage, Univ. of Basilicata, Matera, MT 75100, Italy. Email: mauro.fiorntino@unibas.it

[8]Associate Professor, Dept. of Physics "E.R. Caianiello", Univ. of Salerno, Fisciano, SA 84084, Italy. ORCID: https://orcid.org/0000-0001-7628-8870. Email: fmadonna@unisa.it

[9]Managing Director, Institute of Methodologies for Environmental Analysis, National Research Council, Tito Scalo 85050, Italy. Email: rosa.lasaponara@imaa.cnr.it

Note. This manuscript was submitted on July 3, 2024; approved on September 24, 2024; published online on August 22, 2025. Discussion period open until January 22, 2026; separate discussions must be submitted for individual papers. This paper is part of the ***Journal of Irrigation and Drainage Engineering***, © ASCE, ISSN 0733-9437.

Introduction

The quantification of hydrological components in the soil is crucial for different water resource management applications such as irrigation, drinking water, and industry (Brunner and Simmons 2012). The hydrological variability is predicted to increase with climate change, making predictions for recharge and groundwater storage even more important to implement and to maintain sustainable water use (Vogel 2019). Groundwater is usually the only source of water in arid and semiarid regions due to the low amount of precipitation and lack of surface water resources. Water balance estimation is one of the most sensitive steps in groundwater management, which have a critical component in the commonly known "recharge rate estimation" (Vázquez-Suñé et al. 2006; Spelman et al. 2013).

Most of the soil water processes in agricultural fields occur while the soil is in unsaturated conditions (Hillel 1998). The unsaturated soil is well-known as a complicated porous medium due to its temporally and spatially variable parameters. Consequently, the unsaturated water flow in such condition is hard to measure or simulate, especially when hysteresis (i.e., the dependence of soil water retention curve on whether soil is wetting or draining) and root water uptake are taken into account (Lipiec and Tarkiewicz 1990; Hillel 1998). Recently, unsaturated flow modeling has become one of the most active topics of research in hydrology and soil physics (Simunek et al. 2008; Zhang et al. 2019).

Many models of varying degree of complexity and dimensionality have been developed during the past several decades to quantify the basic physical and chemical processes affecting water flow and pollutant transport in the unsaturated zone (Langergraber and Simunek 2005; Simunek et al. 2005). These models are now being used increasingly for a wide range of applications in research and management of natural subsurface systems. Modeling approaches range from relatively simple analytical and semianalytical models [e.g., SWI (Wagner et al. 1999) and SMAR (Manfreda et al. 2014)] to more complex numerical codes [e.g., HYDRUS (Simunek et al. 2008), MODFLOW-SURFACT (Panday and Huyakorn 2008), STOMP (White et al. 2008), SWAP (van Dam et al. 2008), and TOUGH2 (Finsterle et al. 2008)] that permit consideration of a large number of simultaneous nonlinear processes. Among the various proposed methodologies (Mansell et al. 2002; An et al. 2010; An and Yu 2014), the numerical simulation of transient water flow in saturated–unsaturated porous media carried out using HYDRUS software has been widely used in many different research areas such as drip and pitcher irrigation modeling (Ebrahimian et al. 2013; Mohammad et al. 2014; Yang et al. 2019), root zone and deep vadose zone modeling (Kornelsen and Coulibaly 2014; Zhang et al. 2020), groundwater modeling (Assefa and Woodbury 2013; Vogel 2019), and hydrology (Jandl et al. 2002; Hilten et al. 2008).

Almost all of the abovementioned models require information about the soil moisture status; however, the field measurements of soil moisture and soil characteristics are often time-consuming and require great efforts to adequately sample even small farms making the model with high complexity or requirement to the measured data limited to small scales and research applications (Manfreda et al. 2014). With the advancement of satellite technologies (e.g., passive microwave data, Radar data, etc.) and the production of surface soil moisture data on a daily basis for the entire globe, a very suitable possibility for modeling the soil water balance in the large and small scales has been created. On the one hand, satellite data are only representative of the top 5–10 cm of the top soil maximum; on the other hand, the high volume of calculations and input data of advanced numerical models has greatly limited the possibility of distributed modeling in large scales with them (Wagner et al. 1999; Manfreda et al. 2014; Ragab 1995). The solution to these problems would be to find a robust straightforward relationship between the surface soil moisture and deep soil moisture. While the empirical and semiempirical methods for finding the relationship between the surface and deep soil moisture are limited to the areas they were developed for, the description of an analytical relationship between the soil moisture in the first centimeters of the soil column, hereafter referred to as surface soil moisture (SSM), and the next meters of it, hereafter referred to as deep soil moisture (DSM), has been emphasized as a significant challenge (Ragab 1995; Puma et al. 2005; Sabater et al. 2007; Albergel et al. 2008; Ochsner et al. 2013).

The soil moisture analytical relationship (SMAR) was derived from a simplified soil water balance equation for arid and semiarid environments in the absence of the lateral flow providing a relationship to estimate DSM from the SSM variations (Manfreda et al. 2014). SMAR has some advantages over the aforementioned models making it theoretically robust and practically low-demanding: (1) it has an analytical solution to a robust physical soil water balance equation; (2) it requires a few input parameters and variables; and (3) its parameters can be directly determined knowing the soil texture and climate conditions of the study area. Applications of the SMAR model in estimating the DSM from the time series of in situ and remotely sensed SSM proved its performance in providing a good description of DSM at both local and regional scales [e.g., (Manfreda et al. 2014; Baldwin et al. 2017; Faridani et al. 2017a, b; Gheybi et al. 2019; Zhuang et al. 2020)]. In the original model proposed by Manfreda et al. (2014), the water loss function was assumed to be a linear function of current soil moisture content and maximum water loss in the soil, which is in a way equal to the sum of maximum evapotranspiration and deep percolation. Faridani et al. (2017b) proposed to improve SMAR's performance by assuming a soil water loss function that could account for the nonlinearity of the water loss process, suggesting this modified SMAR (MSMAR) model could estimate other soil hydrological variables.

The aim of this study was, first, to translate the variability observed in SSM into the hydrological constituents of the underlying soil profile through redefining the MSMAR model to produce daily DSM, evapotranspiration (ET), and deep percolation (DP)—within arid and semiarid regions, specifically in scenarios devoid of lateral flow. Second, the study sought to assess and compare these outcomes with those derived from the widely utilized numerical method, HYDRUS-1D, by utilizing field measurements conducted in a sprinkler-irrigated farm situated in northeast Iran.

Materials and Methods

Data and Study Area

For the purpose of this research, the information presented by Naghedifar et al. (2018) was exploited including the soil moisture measurements, meteorological data, soil physical properties, volume of applied irrigation water, and cultivation dates. The study area in this research was a 17-ha farm (F) growing triticale (x *Triticosecale* Wittmack) under sprinkler irrigation and located near Neishabour (58° 39′ 2″ E and 36° 11′ 3″ N), Iran [Figs. 1(a and b)]. Triticale is a hybrid of wheat and rye with maximum rooting depth of 100 cm and soil water depletion fraction of 0.55, which is the average fraction of total available soil water that can be depleted from the root zone before plant water stress (reduction in ET) occurs (Allen et al. 1998). Annual average precipitation and potential evapotranspiration at the experimental site are 247 and 2,335 mm, respectively (Naghedifar et al. 2018). The highest and lowest monthly-averaged precipitations occur in March and August (51 and 0.16 mm, respectively).

The daily soil moisture profile in the study area [Fig. 1(a)], was monitored via five observation wells [Fig. 1(b)] equipped with eight REC time-domain reflectometry (TDR) sensors (Naghedifar et al. 2018) installed down to 3 m to capture the root zone soil moisture variations at a high vertical resolution [Fig. 1(c)]. Several soil samples were obtained whilst drilling each of the observation wells, which were analyzed in the Laboratory of Water Science and Engineering Department of Ferdowsi University of Mashhad to determine the soil parameters and water content of different soil layers in the field. Sensor calibration was performed following the procedure outlined by Cobos and Chambers (2010) and using the regression equation between the calibrated and measured soil water contents ($y = 0.9959x + 0.0007$; $R^2 = 0.947$). These data were also used to set up initial conditions of the models and validate the simulation results. The overall soil water content in the field was then calculated averaging the TDR values obtained from the five monitoring wells (i.e., spatial average). Table 1 summarizes the results of the soil physical properties at the experimental site.

HYDRUS-1D Numerical Model

HYDRUS-1D (Simunek et al. 2005) is a physically based model to solve and couple governing equations of water flow, solute, and heat transport along with root water and nutrient uptake. Water flow in a variably saturated soil in HYDRUS-1D is described by the mixed form of a Richards' equation (Richards 1931)

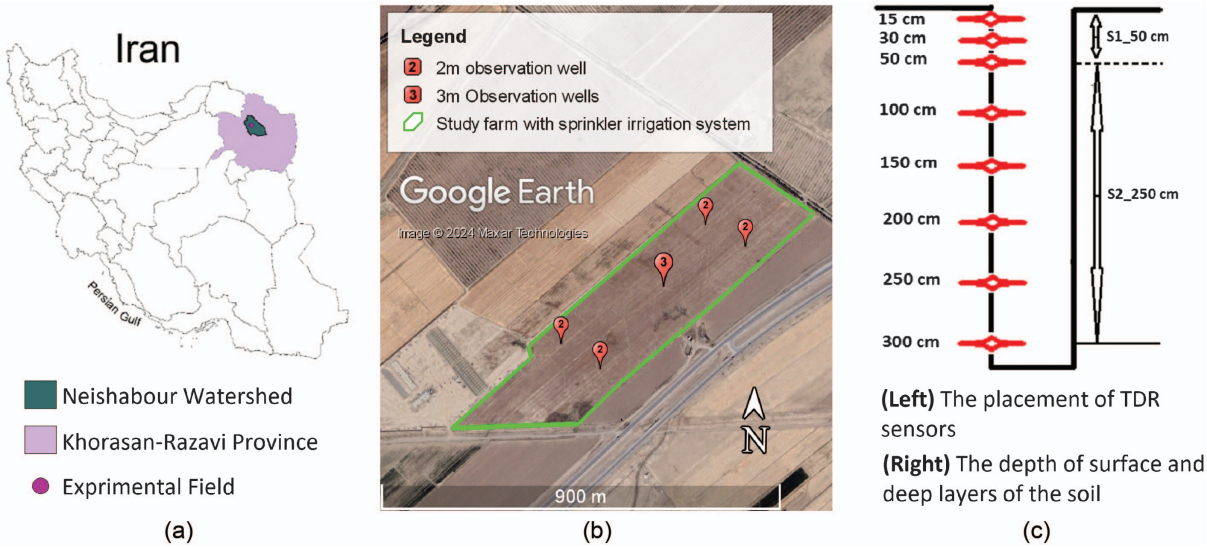

Fig. 1. (Color) (a) Location of study farm in Neishabour watershed; and (b) layout of sprinkler and furrow irrigation systems along with the locations of two- and three-meter-deep monitoring wells. The natural look image was take from Google Earth (base map © Google Earth, Image © 2024 Maxar Technologies). (c) Schematic diagram showing the installation of soil moisture sensors into the monitoring wells (adapted from Naghedifar et al. 2018).

Table 1. Soil physical properties of experimental plots at different layers

Soil depth (cm)	Soil mineral particles (%)			Soil texture	ρb^a (g/cm^3)	SVWC^b (%)	θ_s^c	K_s^d (cm/day)
	Sand	Silt	Clay					
0–50	29.08	30.00	40.92	Clay loam	1.60	42	0.4418	3.84
50–100	44.25	34.65	21.10	Loam	1.52	34	0.3991	9.30
100–150	32.75	35.75	31.50	Clay loam	1.65	41	0.4418	2.81
150–200	61.00	26.75	12.25	Sandy loam	1.50	36	0.387	31.62
200–250	68.50	19.50	12.00	Sandy loam	1.61	32	0.387	28.41
250–300	55.60	24.40	20.00	Sandy loam	1.56	36	0.387	13.99

[a]Bulk density.
[b]Saturated volumetric water content.
[c]The calibrated parameters of van Genuchten's water retention model: soil moisture at saturation point.
[d]The calibrated parameters of van Genuchten's water retention model: hydraulic conductivity at saturation point.

$$\frac{\partial \theta}{\partial t} = \frac{\partial}{\partial z}\left[K(\psi)\frac{\partial \psi}{\partial z} + K(\psi)\right] - \text{RWU} \tag{1}$$

where θ = volumetric water content [L^3L^{-3}]; ψ = soil water pressure head [L]; K = saturated/unsaturated hydraulic conductivity [LT^{-1}]; t = time [T]; z = vertical space coordinate [L]; and RWU = root water uptake [$L^3L^{-3}T^{-1}$]. Thanks to the constitutive relations of soil water retention curve $\theta(\psi)$ and saturated/unsaturated hydraulic conductivity, HYDRUS-1D employs a so-called modified-Picard iteration scheme (Celia et al. 1990) to solve Eq. (1) iteratively. Among different options available in HYDRUS-1D, the following constitutive relations of Van Genuchten (1980) have been used:

$$\theta(\psi) = \theta_r + \frac{\theta_s - \theta_r}{(1 + (\alpha\psi)^{\lambda})^{\phi}} \tag{2}$$

$$K(\psi) = K_s S_e^{\frac{1}{2}}\left(1 - \left(1 - S_e^{\frac{1}{\phi}}\right)^{\phi}\right)^2 \quad \text{where } \phi = 1 - \frac{1}{\lambda}, \quad \lambda > 1 \tag{3}$$

$$S_e = \frac{\theta - \theta_r}{\theta_s - \theta_r} \tag{4}$$

where S_e = effective saturation [L^3L^{-3}]; θ_s and θ_r = saturated and residual water contents, respectively [L^3L^{-3}]; α = inverse of air-entry value [L^{-1}]; ϕ and λ = pore size distribution indices; and K_s = saturated hydraulic conductivity [LT^{-1}]. The root water uptake module of HYDRUS-1D (Šimůnek and Hopmans 2009) employs the following equation to obtain noncompensated actual root water uptake:

$$\text{RWU}(\psi \cdot z \cdot t) = \alpha_s(\psi \cdot z \cdot t)b(z \cdot t)T_p(t) \tag{5}$$

where α_s (ψ, z, t) = stress response function; b = one-dimensional (1D) normalized water uptake distribution function [L^{-1}]; and T_p = potential transpiration rate [LT^{-1}]. In this study, the normalized water uptake distribution function of Hoffman and Van Genuchten (1983) and stress response function of Feddes (1982) have been employed, which are demonstrated by Eqs. (6) and (7)

$$b(z) = \begin{cases} \dfrac{1.6667}{L_R} & z > L - 0.2L_R \\ \dfrac{2.0833}{L_R}\left(1 - \dfrac{L - z}{L_R}\right) & L - L_R < z < L - 0.2L_R \\ 0 & z < L - L_R \end{cases} \quad (6)$$

$$\alpha(h) = \begin{cases} \dfrac{h - h_4}{h_3 - h_4} & h_4 < h \le h_3 \\ 1 & h_3 < h \le h_2 \\ \dfrac{h - h_1}{h_2 - h_1} & h_2 < h \le h_1 \\ 0 & h \le h_4 \, or \, h > h_1 \end{cases} \quad (7)$$

where L = total depth of soil that is intended to be simulated [L]; L_R = maximum root depth [L]; and h_1, h_2, h_3, and h_4 = pressure head threshold parameters [L]. Eq. (1) is a partial differential equation requiring initial condition and two boundary conditions. The initial soil moisture was measured during the experiment by means of soil moisture sensors installed in the observation wells. The lower boundary condition was set as the free drainage boundary, and the upper boundary (at soil surface) was set as the atmospheric boundary condition. This requires the variations of the potential evaporation rate to be specified during the experiment. To this end, the potential evapotranspiration rate (ET_P [LT^{-1}]) was calculated following the recommendations of Allen et al. (1998).

During the iterative process of solving Richards' equation, HYDRUS-1D calculates the distribution of pressure head in the soil profile at each time step. Therefore, water flux q [$L^3L^{-2}T^{-1}$] can be computed at an arbitrary nodal point by discretizing the Darcy–Buckingham equation

$$q = -K(\psi)\frac{d\psi}{dz} \quad (8)$$

where positive and negative fluxes at each node represent upward and downward movement of water in the soil profile, representing ET and DP, respectively.

Modified Soil Moisture Analytical Relationship

Manfreda et al. (2014) presented the SMAR model to define a soil water balance relationship in a two-layered soil profile in which infiltration is the most important flux between the two layers and other processes, such as lateral flow and capillary rise, are assumed negligible. The infiltration is not expressed as a function of precipitation, but as a function of the percentage of soil moisture in the first layer, which allows us to obtain soil moisture in the second layer as a function of soil moisture in the top layer:

$$n_1 Zr_1 y(t) = n_1 Zr_1 y[s_1(t) \cdot t] = n_1 Zr_1 \begin{cases} (s_1(t) - s_{c1}). & s_{c1} < s_1(t) \\ 0. & s_1(t) \le s_{c1} \end{cases} \quad (9)$$

where $y(t)$ = fraction of soil saturation infiltrating into the deep layer; n_1 = soil porosity; Zr_1 [L] = soil depth; $s_1 (= \theta_1/n_1)$ = surface relative saturation; and s_{c1} = value of field capacity relative saturation. From now on the subscripts 1 and 2 in the formula represent the soil's first/surface and second/deep layers, respectively. The flux from the surface layer is only considered significant if the moisture content is higher than the field capacity and it occurs in less than

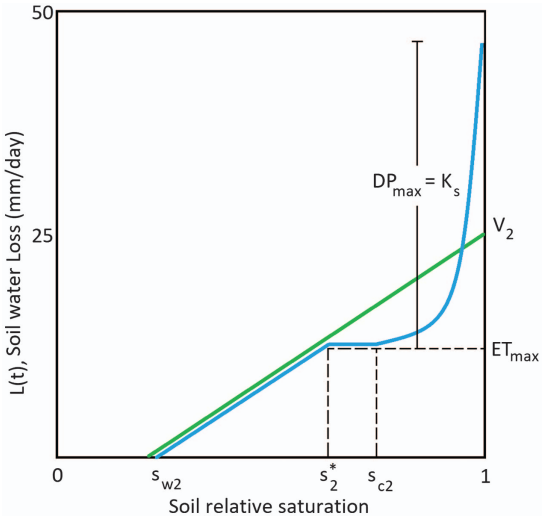

Fig. 2. (Color) Typical water loss function [$L(s)$] of SMAR model (green) and MSMAR model (blue) for the typical climate, soil, and vegetation conditions in arid and semiarid regions.

1 day following the Green–Ampt infiltration relationship (Green and Ampt 1911). By defining $x_2 = (s_2\text{-}s_{w2})/(1\text{-}s_{w2})$ as the effective relative saturation of the soil second layer and $\omega_0 = (1\text{-}s_{w2})n_2 Zr_2$ as the maximum soil water storage, the SMAR soil water balance is described as

$$(1 - s_{w2})n_2 Zr_2 \frac{dx_2(t)}{dt} = n_1 Zr_1 y(t) - V_2 x_2(t) \quad (10)$$

where s_2 = second layer's current relative saturation; s_{w2} = relative saturation at the wilting point; n_2 = soil porosity; Zr_2 [L] = soil depth; V_2 [LT^{-1}] = soil water loss coefficient accounting for both evapotranspiration and percolation losses; and x_2 = effective relative soil saturation of the second soil layer. The second term of the right side of Eq. (10) represents a linear soil water loss function where soil water loss would be linearly reduced from a maximum value at the saturation point to zero at the wilting point (Fig. 2).

Faridani et al. (2017b) presented the MSMAR model by substituting the constant V_2 with a variable coefficient $L(t)$ that estimates a different maximum soil water loss in each day as the sum of potential ET and DP in that day:

$$L(t) = \mathrm{ET}(t) + \mathrm{DP}(t) \quad (11)$$

where at a certain soil saturation in the second layer (s_2), $L(t)$ [LT^{-1}] = total soil water loss; $\mathrm{ET}(t)$ [LT^{-1}] = soil water loss due to evapotranspiration; and $\mathrm{DP}(t)$ [LT^{-1}] = soil water loss due to deep percolation. According to Laio et al. (2001), the maximum DP occurs under saturated conditions and decreases exponentially with decreasing soil hydraulic conductivity from K_s at saturation point to zero at field capacity:

$$\mathrm{DP}(t) = \begin{cases} K_s s_2(t)^c & s_{c2} < s_2(t) \le 1 \\ 0 & s_{w2} < s_2(t) \le s_{c2} \end{cases} \quad (12)$$

where K_s [LT^{-1}] = hydraulic conductivity of soil saturation; and c = empirical parameter of power function. The amount of loss due to evapotranspiration was also calculated from the following equation (Laio et al. 2001):

$$\mathrm{ET}(t) = \begin{cases} \mathrm{ET}_{\max}(t) & s_2^* < s_2(t) \le 1 \\ \mathrm{ET}_w + (\mathrm{ET}_{\max}(t) - \mathrm{ET}_w)\dfrac{s_2(t) - s_{w2}}{s^* - s_{w2}} & s_{w2} < s_2(t) \le s_2^* \end{cases} \tag{13}$$

where s_{w2} = second layer's saturation degree at the wilting point; s^* = saturation degree at the stomata closure; $\mathrm{ET}_{\max}$ [LT^{-1}] = daily potential evapotranspiration; and ET_w [LT^{-1}] = evapotranspiration at the wilting point. The water loss function of the MSMAR can be compared with that of SMAR in Fig. 2. In this regard, $L_2(t)$ can be replaced with V_2 to account for nonlinearity of the soil water loss, and Eq. (11) becomes

$$(1 - s_{w2})n_2 Zr_2 \frac{dx_2}{dt} = n_1 Zr_1 y(t) - L_2(t)x_2(t) \tag{14}$$

Eq. (14) can be redefined using the coefficients a and b as follows:

$$a = \frac{L(t)}{(1 - s_{W2})n_2 Zr_2} \cdot b = \frac{n_1 Zr_1}{(1 - s_{W2})n_2 Zr_2} \tag{15}$$

The value of these parameters can be directly related to the depth of the two layers and the soil water loss coefficient. As a result, the soil water balance relationship becomes

$$\frac{dx_2(t)}{dt} = by(t) - ax_2(t) \tag{16}$$

Assuming an initial condition for relative saturation $x_2(t)$ equal to zero, the analytical solution for this linear differential equation is

$$x_2(t) = \int_0^t be^{a(t'-t)}y(t')dt' \tag{17}$$

For practical applications, the relationship can be represented discretely:

$$x_2(t_j) = \sum_{i=0}^{j} be^{a(t_i - t_j)}y(t_i)dt \tag{18}$$

Assuming $\Delta t = [t_{(j)} - t_{(j\text{-}1)}]$ and extending Eq. (18), the following equation is obtained for soil moisture in the second layer based on the time series of surface soil moisture:

$$x_2(t_j) = x_2(t_{j-1})e^{-a(t_j - t_{j-1})} + by(t_j)(t_j - t_{j-1}) \tag{19}$$

And it can be rewritten as a function of s_2 as follows:

$$s_2(t_j) = s_{w2} + (s_2(t_{j-1}) - s_{w2})e^{-a(t_j - t_{j-1})} + (1 - s_{w2})by(t_j)(t_j - t_{j-1}) \tag{20}$$

The main parameters of MSMAR include Zr_1, Zr_2, n_1, n_2, s_{c1}, s_{c2}, s_2^*, s_{w2}, K_s, c, $\mathrm{ET}_{\max}$, and ET_w. Since there is a clear physical meaning to each parameter, they can be determined according to the soil texture using reference tables in the literature (e.g., Laio et al. 2001; Manfreda et al. 2014; Faridani et al. 2017b) or can be calibrated based on the field data. In the case of $\mathrm{ET}_{\max}$ and ET_w, they can be determined based on the climatic conditions of the study area.

Data Refactoring and Calibration

HYDRUS-1D can calculate most of its outputs (i.e., DSM and DP) at each node of the mesh created from the whole soil column; however, MSMAR's outputs represent the overall estimate of the whole second layer of soil. Therefore, the outputs from both models as well as TDR measurements should be refactored in a way that they represent the same concept. In this regard, the weighted average of the TDR measurements and HYDRUS-1D DSM estimates according to their representing depth should be calculated [see Fig. 1(c)]. The resulted values should then be divided by the second layer porosity (n_2) to represent the soil relative saturation as MSMAR does. For example, the average relative saturation of a soil column with 100 cm depth (i.e., 15 cm of surface layer + 85 cm of second layer) is calculated as $\mathrm{s2}_{100\ \mathrm{cm}} = 1/n_2[(15/85) \times \theta_{30\ \mathrm{cm}} + (20/85) \times \theta_{50\ \mathrm{cm}} + (50/85) \times \theta_{30\ \mathrm{cm}}]$.

The DP estimates of MSMAR and HYDRUS-1D refer both to the same concept, which is the water amount passed through a certain depth in the soil, so there is no need for change. In the case of actual evapotranspiration (ET_a), HYDRUS-1D estimates the amount of ET_a as a function of crop coefficient and independent from the SM status, whereas MSMAR estimates it as a function of SM status. In other words, HYDRUS-1D produces only one ET_a with which all MSMAR ET_a values must be compared.

In order to calibrate HYDRUS-1D, the initial guess for soil hydraulic parameters can be obtained using RETC (Leij et al. 1992) and ROSETTA (Schaap et al. 2001) software based on the soil texture measurements (Table 1). These values can then be fine-tuned in the calibration phase to improve the accuracy of simulations. Root water uptake parameters of Feddes' function (Feddes 1982) can be selected from Wesseling et al. (1991).

The MSMAR' parameters can be calibrated using a genetic algorithm in the MATLAB software (The MathWorks, n.d.) with the objective function of minimum root mean square error (RMSE) between the observed and estimated values assuming the lower boundary (LB) and upper boundary (UB) conditions according to the soil and climatic characteristics.

Upon data refactoring, the MSMAR model can undergo two calibration schemes to understand how the MSMAR performed compared to the measured data and to the numerical simulations. These two calibration schemes aim at minimizing the RMSE between the MSMAR estimates and two sets of reference data: (1) measured TDR values; and (2) HYDRUS-1D outputs (i.e., SM, ET, and DP), respectively. Ideally, the first calibration scheme should have incorporated actual DP and ET measurements, potentially obtained via field installations such as Lysimeters; however, only TDR measurements were available due to the constraints.

Results

HYDRUS-1D and MSMAR models were calibrated following the instructions in the section "Data Refactoring and Calibration" for a triticale field in Iran. Table 2 provides the calibrated parameters for each calibration scheme as well as the UBs and LBs of the MSMAR parameters based on the Table 1. The remaining MSMAR parameters of Eq. (13) (i.e., ET_w and $\mathrm{ET}_{\max}$) were assumed to be equal to a constant daily value (0.001 cm/day) and daily potential evapotranspiration (ET_p) estimated by FAO dual crop coefficient method (see section 3.2), respectively. In the next step, both models simulated the soil water balance parameters (i.e., SM, ET, and DP) of the triticale field for a period of six months starting from sowing to harvest date (November 1, 2012 through April 22, 2013). For HYDRUS-1D, the rooting depth of the triticale was assumed to be 1 m and the effect of salinity was assumed to be negligible since soil and water quality samples in the region showed average salinity values of 2.89 and 2.24 $\mathrm{dS \cdot m^{-1}}$, respectively.

Table 2. MSMAR boundary conditions and calibrated parameters for different calibration schemes and soil depths using GA in MATLAB based on the minimum RMSE

Boundary conditions	Soil depth (cm)	s_{c1}[a]	s_{w2}[b]	s_{c2}[c]	n_1[d]	n_2[e]	K_s[f] (cm/day)	c[g]	s_2^*[h]
UB[i]	30–50	0.8	0.45	0.8	0.445	0.445	6	26	0.73
LB[j]	30–50	0.6	0.35	0.6	0.440	0.380	4	11	0.55
UB	100–300	0.8	0.45	0.8	0.445	0.470	17	26	0.73
LB	100–300	0.6	0.25	0.6	0.440	0.380	4	11	0.53
MSMAR calibration									
Scheme 1.	30	0.630	0.447	0.792	0.443	0.434	5.997	11.009	0.723
Minimum RMSE between	50	0.613	0.445	0.796	0.441	0.421	5.988	11.184	0.726
MSMAR's DSM and TDR data	100	0.688	0.449	0.769	0.442	0.415	16.936	13.347	0.705
	150	0.787	0.326	0.690	0.442	0.416	16.892	11.562	0.617
	200	0.798	0.266	0.685	0.442	0.386	16.986	11.013	0.602
	250	0.600	0.449	0.799	0.440	0.470	16.836	23.543	0.729
	300	0.800	0.250	0.602	0.445	0.381	16.998	11.002	0.531
Scheme 2.	30	0.788	0.450	0.610	0.443	0.401	4.003	25.980	0.578
Minimum RMSE between the ensemble of	50	0.785	0.417	0.619	0.442	0.390	4.006	25.894	0.579
HYDRUS-1D's and MSMAR's DSM,	100	0.792	0.263	0.786	0.443	0.383	4.002	25.976	0.681
ET and DP results.	150	0.793	0.295	0.747	0.441	0.383	4.004	25.971	0.657
	200	0.755	0.298	0.746	0.445	0.381	4.004	25.949	0.657
	250	0.800	0.251	0.800	0.444	0.380	4.000	26.000	0.690
	300	0.767	0.261	0.754	0.441	0.382	4.008	25.971	0.655

[a]Relative soil saturation of the first layer at field capacity.
[b]Relative soil saturation of the second layer at the wilting point.
[c]Relative soil saturation of the second layer at field capacity.
[d]Soil porosity of the first layer.
[e]Soil porosity of the second layer.
[f]Saturated hydraulic conductivity of the second soil layer.
[g]Empirical parameter for the power function.
[h]Relative soil saturation at stomata closure for the second layer.
[i]Upper boundary condition.
[j]Lower boundary condition.

Soil Moisture Status

The first TDR installed under soil surface assumed to represent the surface layer of MSMAR model [$Zr_1 = 15$ cm, Fig. 1(c)], and its measurements were used to calculate SSM and infiltration from the first to the second layer in Eq. (9). Figs. 3(a–g) illustrate the SM time series for a soil column with different depths (30, 50, 100, 150, 200, 250, and 300 cm) calculated by the MSMAR and HYDRUS-1D as well as the TDR measurements. As explained in the section "Data Refactoring and Calibration," the values in Fig. 3 were refactored to represent the average SM status for the soil column with specific depth. Fig. 3(h) illustrates the precipitation and irrigation events during the study period. Since such soil recharging events were very important to the performance of MSMAR (Manfreda et al. 2014; Faridani et al. 2017a, b; Gheybi et al. 2019), and since the TDR data were missing during some of these events, it was assumed that the precipitation and irrigation events greater than 15 mm could reach the surface layer to the saturation state (i.e., $s_1 = 1$).

Fig. 3 shows that the precipitation and irrigation events could effectively recharge the soil profile to the field capacity ($\approx$0.8) down to the triticale root zone (100 cm). For the HYDRUS-1D model, the variation and magnitude of soil saturation decreased dramatically beneath the root zone ($Zr_2 > 100$ cm) indicating the significance of considering the root water uptake in this model, whereas the DSM decreased more gradually and reached to a steady state in $Zr_2 > 200$ cm for the MSMAR model as a result of not considering directly the root water uptake into account. The MSMAR DSM-30cm time series in Fig. 3(a) exhibited a charging/discharging pattern after the infiltration event unlike the deeper depths [Figs. 3(b–g)]. This normally happens when the fraction of soil water infiltrated into the lower layer [$y(t)$ in Eq. (9)] is bigger than the total soil water losses [L (t) in Eq. (11)], so the process of depleting the soil would last for a few days.

For quantitative interpretations, Table 3 presents statistical errors (percentage of average root mean square error, RMSE%) and correlation (coefficient of determination, R^2) indices between the DSM estimated by the MSMAR and HYDRUS-1D models. Since the RMSE has the same unit of the study parameter, the magnitude of data affects the magnitude the RMSE. Given the varying magnitude of DSM along the soil column, the statistical indices needed to be unit-less (i.e., normalized) for comparative purposes. Hence, the RMSE for each depth was divided by the average of DSM values at that depth to express it as a percentage (RMSE%).

The first and second rows of Table 3 show the performance of MSMAR and HYDRUS-1D when both calibrated and compared with the TDRs. The results showed that both models had the best DSM estimates with a 100 cm soil column and that MSMAR had higher performance than HYDRUS-1D in estimating DSM in all depths in terms of higher R^2 and lower RMSE%. The third and fourth rows of Table 3 show the performances of MSMAR when calibrated with the TDRs and HYDRUS-1D, respectively, and in comparison with the HYDRUS-1D's DSM results. The calibration criterion in the fourth row was to produce the minimum RMSE among all the produced variables by the two models (i.e., SM, DP, and ET), and the results showed that MSMAR produced much more correlated (bigger R^2) and slightly more accurate (smaller RMSE%) results to those of the HYDRUS-1D. The best performances of MSMAR when calibrated with the TDRs and HYDRUS-1D results were in 50 and 100 cm soil columns, respectively.

Evapotranspiration

In order to estimate the potential evapotranspiration (ET_P), the FAO dual crop coefficient method was employed because of its performance on a daily basis as a result of a dynamic soil

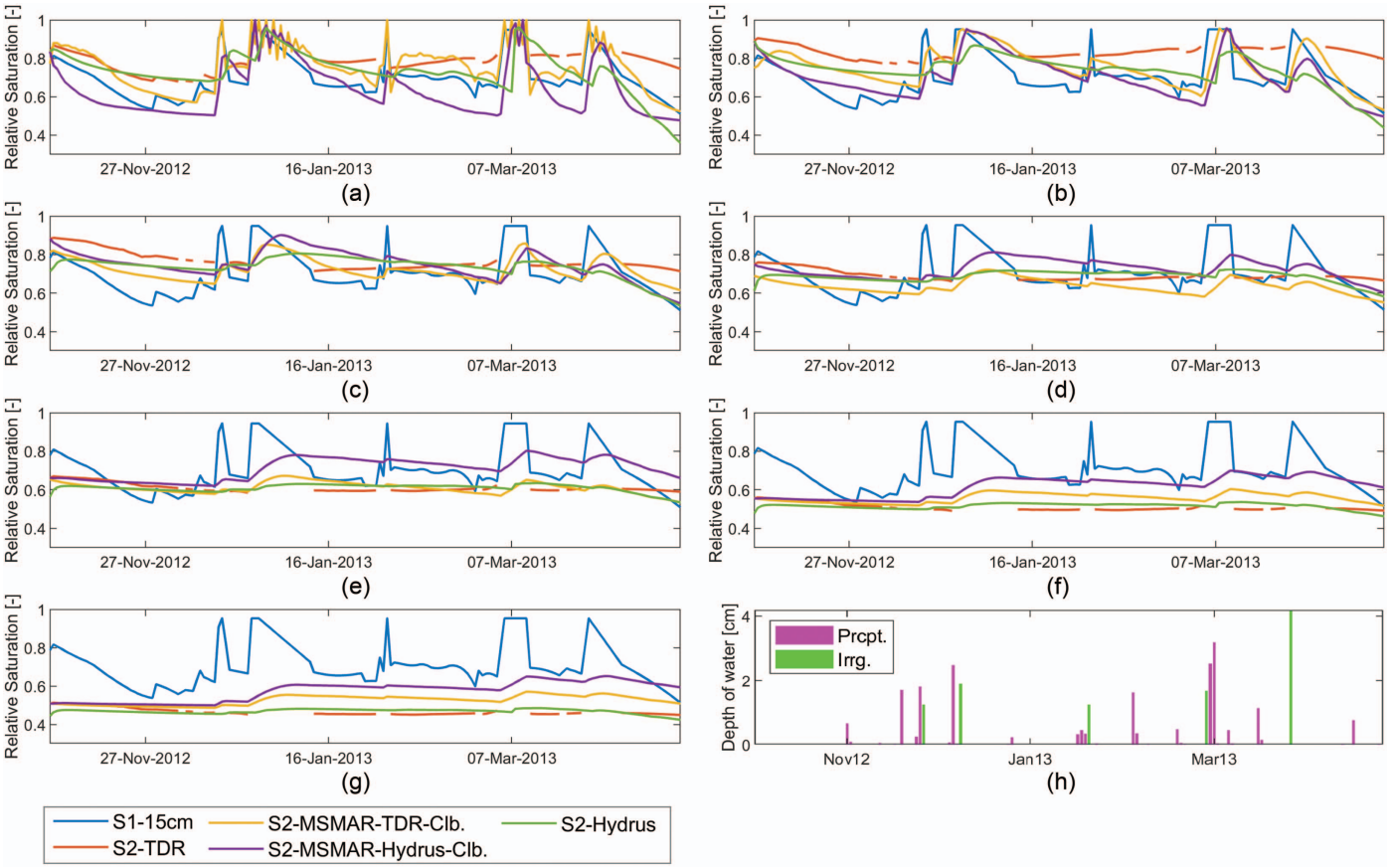

Fig. 3. (Color) Time series of relative saturation in a soil column with the depth of (a) 30 cm; (b) 50 cm; (c) 100 cm; (d) 150 cm; (e) 200 cm; (f) 250 cm; and (g) 300 cm, including a 15 cm hypothetical surface layer for MSMAR. (h) Bar cart of the precipitation and irrigation events. (Blue) surface layer's TDR measurements; (red) deep layer's refactored TDRs; (yellow) MSMAR's DSM estimates calibrated with the TDRs; (purple) MSMAR's DSM estimates calibrated with the HYDRUS-1D results; and (green) HYDRUS-1D's DSM estimates.

Table 3. RMSE and R^2 values between the SM estimates of Hydrus-1D and MSMAR

DSM estimated, calibrated, and validated by	Statistical index	Root zone depths (cm)						
		30	50	100	150	200	250	300
HYDRUS_TDR_TDR	RMSE%	0.130	0.136	0.087[a]	0.078	0.132	0.251	0.290
	R^2	0.048	0.063	0.077[a]	0.028	0.034	0.028	0.022
MSMAR_TDR_TDR	RMSE%	0.099	0.109	0.061[a]	0.057	0.050	0.107	0.142
	R^2	0.362	0.068	0.267[a]	0.059	0.069	0.140	0.390
MSMAR_TDR_HYD	RMSE%	0.654	0.607[a]	0.752	0.807	0.838	0.339	0.775
	R^2	0.324	0.578[a]	0.409	0.629	0.709	0.340	0.117
MSMAR_HYD_HYD	RMSE%	0.769	0.925	1.086[a]	1.074	1.036	0.986	0.870
	R^2	0.448	0.696	0.839[a]	0.627	0.119	0.025	0.002

[a]Best performance of the model considering different depth of the soil column.

evaporation coefficient rather than an average value (Tolk and Howell 2001). Allen et al. (1998) also reported that after precipitations or irrigations, the dual crop coefficient approach had better ET estimations. In the current study, the data provided by Allen et al. (1998) and field observations were used to specify crop coefficient values and length of four growth stages. i.e., initial, crop development, mid-season, and late season stages. The basal crop coefficient values of mid-season and late season were then adjusted for local climatic conditions and the mean plant height at each stage. The variation of plant height was estimated using Richards' function (Richards 1959), which is a well-known S-shaped function commonly used for modeling plant growth. The initial value of plant height at sowing time (November 1, 2012) was set to zero. The function asymptotically approached to the maximum plant height, which was assumed to be 1 m herein for triticale. Table 4 shows the adjusted crop coefficients and the length of each growth stage used in this study, and Fig. 4 illustrates the time series of ET_p in the Triticale study farm calculated by the FAO dual coefficient method (Allen et al. 1998).

HYDRUS-1D computed the actual evaporation and transpiration separately at the upper boundary of soil profile governed by atmospheric condition, and the sum of these parameters produced daily actual evapotranspiration (ET_a). Actual transpiration was calculated by integrating nodal actual root water uptake [Eq. (5)] at

Table 4. Crop coefficient values and length of growth stages for Triticale

Crop	Crop coefficient (K_{cb})			Length of growth stages (day)			
	$K_{cb\,ini}$	$K_{cb\,\mathrm{mid}}$	$K_{cb\,\mathrm{end}}$	L_{ini}	L_{dev}	L_{mid}	L_{late}
Triticale	0.5	1.16	0.25	30	120	60	30

each time step over the root zone. However, MSMAR calculated ET_a following Eq. (13), assuming $Zr_2 = 30$, 50, 100, 150, 200, 250, and 300 cm [Figs. 4(a–c)]. According to Fig. 4, ET_p rises at the beginning of spring due to the increase in the solar radiation, resulting in the depletion of soil water content (S_2). ET_a estimated by HYDRUS-1D and MSMAR followed the same pattern with a distance from ET_p resulting from water deficit in the soil. In the absence of daily ET_p data, MSMAR can assume a constant value for $ET_{\max}$ in Eq. (13) according to the climatic conditions of the study area or based on the calibration for the whole study period, which would obviously provide less accurate results in comparison with the current approach of calculation daily $ET_{\max} (= ET_p)$.

The RMSE% and R^2 values between the ET estimates of HYDRUS-1D and MSMAR when calibrated with the TDRs and HYDRUS-1D results are presented in Table 5. As explained earlier, the ET_a estimates of the models were compared with each other due to the lack of field data. Since both models estimate ET_a as a fraction of daily ET_p, the correlation values (R^2) were naturally high, meaning that RMSE% was more important in determining the performance. According to Table 5, the MSMAR model had its best performance when calibrated with the TDRs and HYDRUS-1D results in 50 and 100 cm soil columns, respectively.

Deep Percolation

HYDRUS-1D estimates DP at each control volume by means of Darcy–Buckingham flux using pressure head distribution obtained

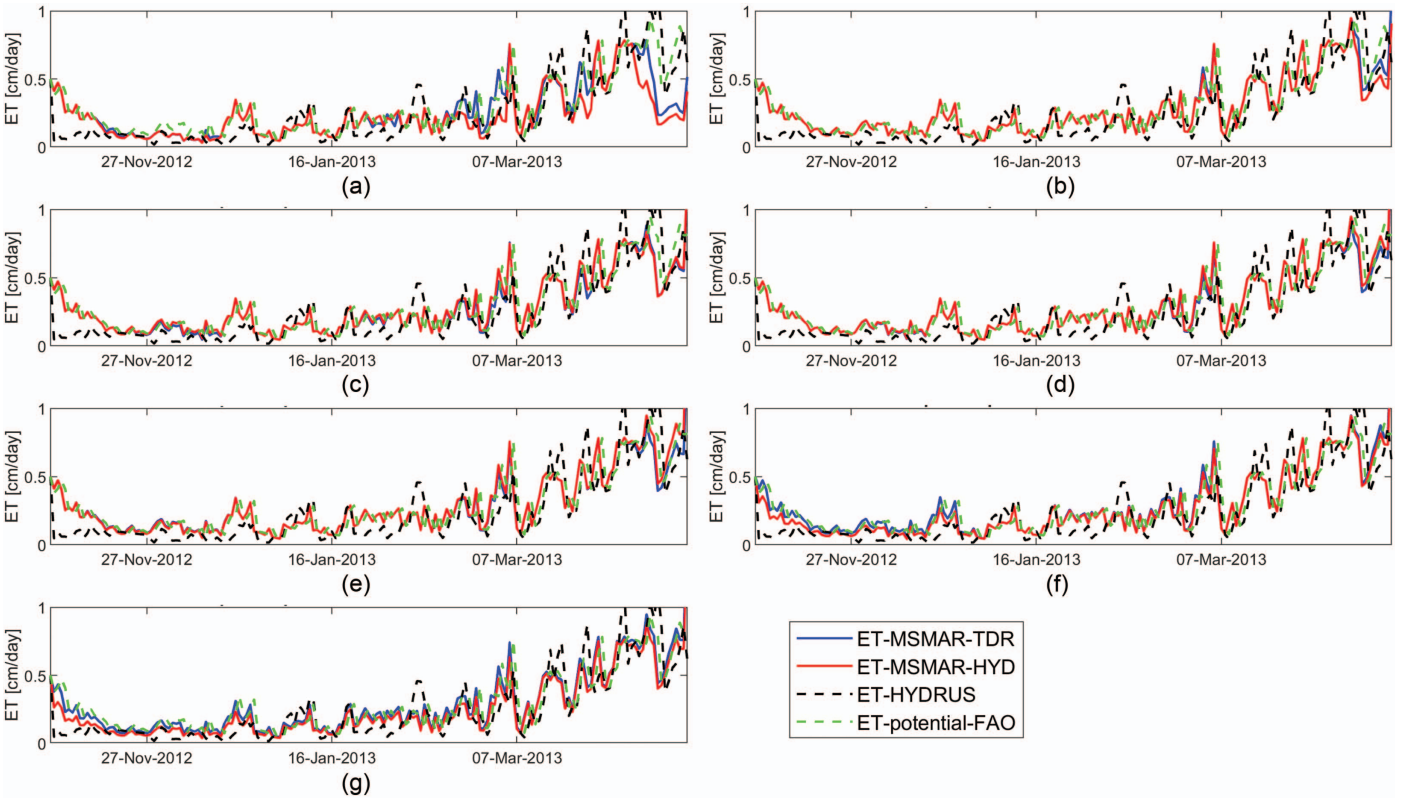

Fig. 4. (Color) Time series of daily actual evapotranspiration (ET_a) in a soil column with the depth of (a) 30 cm; (b) 50 cm; (c) 100 cm; (d) 150 cm; (e) 200 cm; (f) 250 cm; and (g) 300 cm, including a hypothetical surface layer with 15 cm depth for the MSMAR. (Blue) MSMAR's ET_a estimates calibrated with the TDRs; (red) MSMAR's ET_a estimates calibrated with the HYDRUS-1D results; (black) HYDRUS-1D's ET_a estimates; and (green) potential evapotranspiration (ET_p) calculated by FAO dual crop coefficient method.

Table 5. RMSE% and R^2 values between the ET_a estimates of Hydrus-1D and MSMAR

DP estimated, calibrated, and validated by	Statistical index	DP estimated by MSMAR for different root zone depths						
		30	50	100	150	200	250	300
MSMAR_TDR_HYD	RMSE%	0.499	0.387[a]	0.396	0.398	0.403	0.435	0.427
	R^2	0.587	0.744[a]	0.733	0.739	0.734	0.731	0.736
MSMAR_HYD_HYD	RMSE%	0.593	0.411	0.0001[a]	0.411	0.448	0.0001	0.0001
	R^2	0.457	0.704	0.725[a]	0.742	0.724	0.739	0.739

[a]Best performance of the model considering different depth for the soil column.

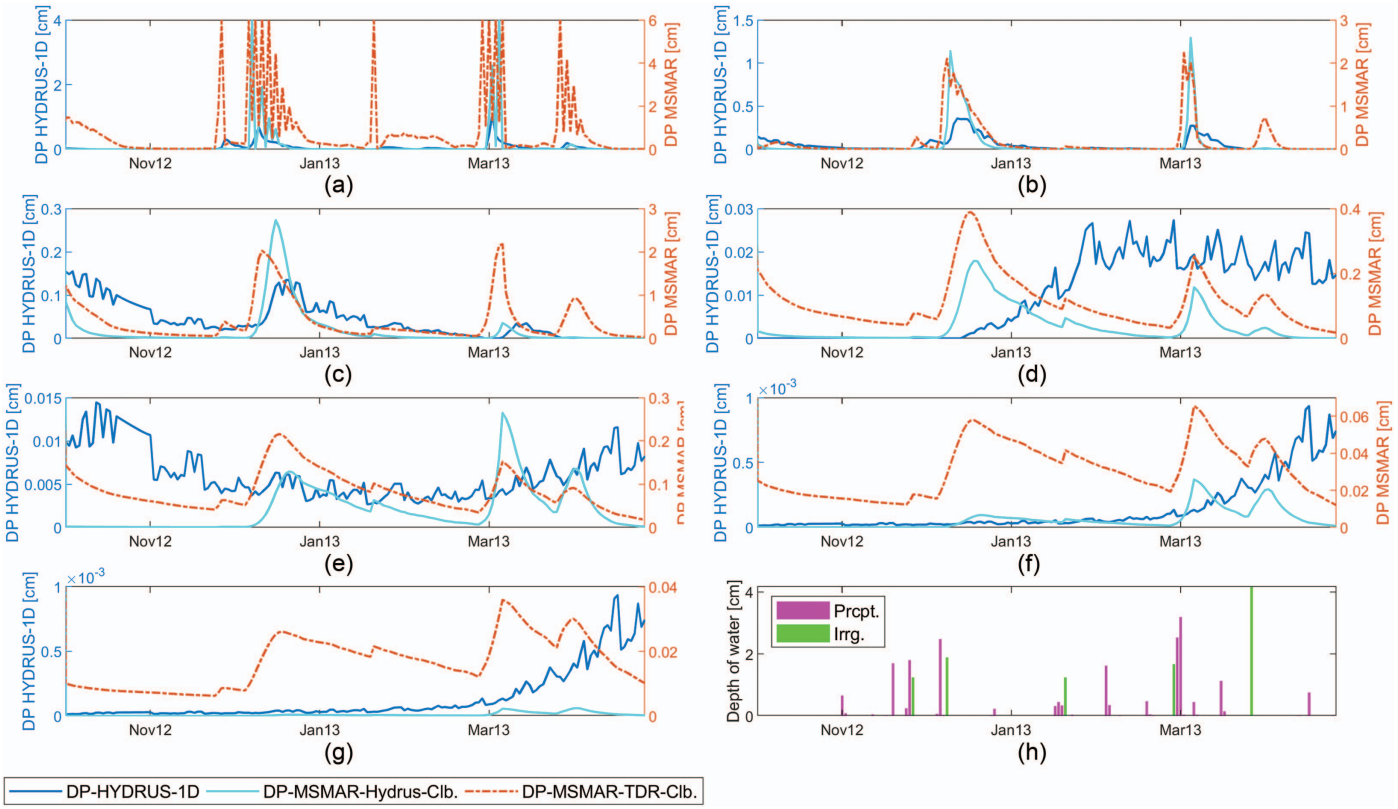

Fig. 5. (Color) Time series of daily deep percolation (DP) in a soil column with the depth of (a) 30 cm; (b) 50 cm; (c) 100 cm; (d) 150 cm; (e) 200 cm; (f) 250 cm; and (g) 300 cm, including a hypothetical surface layer with 15 cm depth for the MSMAR. (Blue) HYDRUS-1D's DP estimates; (red) MSMAR's DP estimates calibrated with the TDRs; and (cyan) MSMAR's DP estimates calibrated with the HYDRUS-1D results. (h) Bar cart of the precipitation (magenta) and irrigation (green) events.

at each time step, while MSMAR estimates this parameter as a function of water content and hydraulic conductivity of the whole second layer of soil following Eq. (12). Figs. 5(a–g) represent the estimated DP by HYDRUS-1D and MSMAR models for different soil column depths (30, 50, 100, 150, 200, 250, and 300 cm).

According to Fig. 5, the DP estimates of HYDRUS-1D and MSMAR had consistent trends down to 100 cm deep; however, the orders of magnitude for the DP estimates were different for the models. HYDRUS-1D's DP estimates became negligible (DP < 1 mm) below the Triticale root depth (1 m), showing the effect of considering root water uptake by the model, whereas MSMAR's DP estimates became negligible with a gradual manner and after 200 cm.

Table 6 represent the RMSE% and R^2 values between the DP estimates of HYDRUS-1D and MSMAR when calibrated with the TDRs and HYDRUS-1D. According to Table 6, MSMAR had its best performance with 50 cm of soil in both calibration schemes; nevertheless, the performance of MSMAR for 100 cm of soil improved a lot and became pretty much close to that of 50 cm when MSMAR was calibrated with the HYDRUS-1D results.

Discussion

The calibration of the HYDRUS-1D and MSMAR models for a triticale field in Iran, as per the instructions in section 2.4, showcases the models' flexibility to adapt to specific agricultural settings. The calibrated models simulated soil water balance parameters over a six-month period, affirming that significant precipitation and irrigation events recharge the soil profile to field capacity down to the root zone. This observation supports the models' assumptions and calibration strategies.

The MSMAR DSM-30 cm time-series displayed a charging/discharging pattern after infiltration events, indicative of a dynamic soil moisture response crucial for accurate soil water balance modeling. A notable observation from the HYDRUS-1D model

Table 6. RMSE% and R^2 values between the DP estimates of Hydrus-1D and MSMAR

DP estimated, calibrated, and validated by	Statistical index	DP estimated by MSMAR for different root zone depths						
		30	50	100	150	200	250	300
MSMAR_TDR_HYD	RMSE%	30.742	8.522[a]	14.054	13.940	15.644	374.231	56.695
	R^2	0.163	0.391[a]	0.089	0.077	0.002	0.003	0.342
MSMAR_HYD_HYD	RMSE%	8.500	2.970[a]	1.358	4.128	6.142	280.355	51.165
	R^2	0.293	0.537[a]	0.239	0.008	0.007	0.002	0.459

[a]Best performance of the model considering different depth for the soil column.

was the dramatic decrease in soil saturation beneath the root zone, underscoring the importance of root water uptake in soil moisture simulations. This could be an area of improvement for the MSMAR model, which did not directly consider root water uptake and showed a more gradual decrease in soil moisture.

The FAO dual crop coefficient method was employed for potential evapotranspiration estimation, with crop coefficient values tailored to local climatic conditions. HYDRUS-1D's separate computation of actual evaporation and transpiration, compared to MSMAR's aggregated approach, could have significant implications for water management practices.

MSMAR's superior performance in estimating DSM across the soil column depths ranging 50 to 100 cm, as indicated by higher R^2 and lower RMSE%, suggests its reliability for soil moisture prediction in the most crop root zone. However, the reasons behind MSMAR's enhanced performance could be further explored.

Conclusions

The MSMAR model offers a robust and efficient approach, utilizing minimal inputs such as surface soil moisture time series, soil texture, and potential evapotranspiration. Its adaptability makes it well-suited for integrating satellite data, facilitating large-scale analyses with significant implications for various environmental applications.

This study demonstrates MSMAR's ability to derive critical hydraulic components of a 100 cm deep soil layer across varied spatial scales. By utilizing in situ or remotely sensed surface soil moisture data, the model provides detailed insights into soil moisture, evapotranspiration, and deep percolation. This capability is particularly valuable for agricultural and water resource management, especially in developing countries and regions lacking extensive gauging networks. Furthermore, coupling the MSMAR model with other distributed hydrological models such as SWAT or MODFLOW can enhance its ability to simulate both saturated and unsaturated soil zones. However, the model is specifically designed for arid and semiarid environments and does not account for lateral underground flow.

Improving model parameters, integrating additional field data, and exploring various soil and climatic conditions will increase the model's applicability across different landscapes. This comparative analysis highlights MSMAR's strengths and limitations in simulating soil water dynamics, emphasizing the importance of calibration strategies in ensuring model accuracy and supporting its use in agricultural and hydrological research.

Data Availability Statement

All data, models, and code generated or used during the study appear in the published article.

References

Albergel, C., C. Rüdiger, T. Pellarin, J.-C. Calvet, N. Fritz, F. Froissard, D. Suquia, A. Petitpa, B. Piguet, and E. Martin. 2008. "From near-surface to root-zone soil moisture using an exponential filter: An assessment of the method based on in-situ observations and model simulations." *Hydrol. Earth Syst. Sci.* 12 (6): 1323–1337. https://doi.org/10.5194/hess-12-1323-2008.

Allen, R. G., L. S. Pereira, D. Raes, and M. Smith. 1998. *Crop evapotranspiration—Guidelines for computing crop water requirements*. FAO irrigation and drainage paper 56. Rome: Food and Agriculture Organization of the United Nations.

An, H., Y. Ichikawa, Y. Tachikawa, and M. Shiiba. 2010. "Three-dimensional finite difference saturated-unsaturated flow modeling with nonorthogonal grids using a coordinate transformation method." *Water Resour. Res.* 46 (11): W11521. https://doi.org/10.1029/2009WR009024.

An, H., and S. Yu. 2014. "Finite volume integrated surface-subsurface flow modeling on nonorthogonal grids." *Water Resour. Res.* 50 (3): 2312–2328. https://doi.org/10.1002/2013WR013828.

Assefa, K. A., and A. D. Woodbury. 2013. "Transient, spatially varied groundwater recharge modeling." *Water Resour. Res.* 49 (8): 4593–4606. https://doi.org/10.1002/wrcr.20332.

Baldwin, D., S. Manfreda, K. Keller, and E. Smithwick. 2017. "Predicting root zone soil moisture with soil properties and satellite near-surface moisture data across the conterminous United States." *J. Hydrol.* 546 (Mar): 393–404. https://doi.org/10.1016/j.jhydrol.2017.01.020.

Brunner, P., and C. T. Simmons. 2012. "HydroGeoSphere: A fully integrated, physically based hydrological model." *Ground Water* 50 (2): 170–176. https://doi.org/10.1111/j.1745-6584.2011.00882.x.

Celia, M. A., E. T. Bouloutas, and R. L. Zarba. 1990. "A general mass-conservative numerical solution for the unsaturated flow equation." *Water Resour. Res.* 26 (7): 1483–1496. https://doi.org/10.1029/WR026i007p01483.

Cobos, D., and C. Chambers. 2010. *Calibrating* ECH_2O *soil moisture sensors, application note*. Pullman, WA: Decagon Devices.

Ebrahimian, H., A. Liaghat, M. Parsinejad, E. Playán, F. Abbasi, and M. Navabian. 2013. "Simulation of 1D surface and 2D subsurface water flow and nitrate transport in alternate and conventional furrow fertigation." *Irrig. Sci.* 31 (3): 301–316. https://doi.org/10.1007/s00271-011-0303-3.

Faridani, F., A. Farid, H. Ansari, and S. Manfreda. 2017a. "Estimation of the root-zone soil moisture using passive microwave remote sensing and SMAR model." *J. Irrig. Drain. Eng.* 143 (1): 04016070. https://doi.org/10.1061/(ASCE)IR.1943-4774.0001115.

Faridani, F., A. Farid, H. Ansari, and S. Manfreda. 2017b. "A modified version of the SMAR model for estimating root-zone soil moisture from time-series of surface soil moisture." *Water SA* 43 (3): 492–498. https://doi.org/10.4314/wsa.v43i3.14.

Feddes, R. A. 1982. *Simulation of field water use and crop yield*. Wageningen, Netherlands: Pudoc.

Finsterle, S., C. Doughty, M. Kowalsky, G. Moridis, L. Pan, T. Xu, Y. Zhang, and K. Pruess. 2008. "Advanced vadose zone simulations using TOUGH." *Vadose Zone J.* 7 (2): 601–609. https://doi.org/10.2136/vzj2007.0059.

Gheybi, F., P. Paridad, F. Faridani, A. Farid, A. Pizarro, M. Fiorentino, and S. Manfreda. 2019. "Soil moisture monitoring in Iran by implementing satellite data into the root-zone SMAR model." *Hydrology* 6 (2): 44. https://doi.org/10.3390/hydrology6020044.

Green, W. H., and G. Ampt. 1911. "Studies on soil phyics." *J. Agric. Sci.* 4 (1): 1–24. https://doi.org/10.1017/S0021859600001441.

Hillel, D. 1998. *Environmental soil physics: Fundamentals, applications, and environmental considerations*. Burlington, NJ: Elsevier.

Hilten, R. N., T. M. Lawrence, and E. W. Tollner. 2008. "Modeling stormwater runoff from green roofs with HYDRUS-1D." *J. Hydrol.* 358 (3–4): 288–293. https://doi.org/10.1016/j.jhydrol.2008.06.010.

Hoffman, G. J., and M. T. Van Genuchten. 1983. "Soil properties and efficient water use: Water management for salinity control." In *Limitations to efficient water use in crop production*, 73–85. Madison, WI: American Society of Agronomy.

Jandl, R., H. Spögler, J. Simunek, and L. K. Heng. 2002. "Simulation of soil hydrology and establishment of a nitrogen budget of a mountain forest." Supplement, *Environ. Sci. Pollut. Res.* 9 (S2): 42–45. https://doi.org/10.1007/BF02987477.

Kornelsen, K. C., and P. Coulibaly. 2014. "Root-zone soil moisture estimation using data-driven methods." *Water Resour. Res.* 50 (4): 2946–2962. https://doi.org/10.1002/2013WR014127.

Laio, F., A. Porporato, C. Fernandez-Illescas, and I. Rodriguez-Iturbe. 2001. "Plants in water-controlled ecosystems: Active role in hydrologic processes and response to water stress: IV. Discussion of real cases." *Adv. Water Resour.* 24 (7): 745–762. https://doi.org/10.1016/S0309-1708(01)00007-0.

Langergraber, G., and J. Simunek. 2005. "Modeling variably saturated water flow and multicomponent reactive transport in constructed wetlands." *Vadose Zone J.* 4 (4): 924–938. https://doi.org/10.2136/vzj2004.0166.

Leij, F. J., M. T. van Genuchten, S. Yates, W. Russell, and F. Kaveh. 1992. "RETC: A computer program for analyzing soil water retention and hydraulic conductivity data." In *Indirect methods for estimating the hydraulic properties of unsaturated soils*, 263–272. Riverside, CA: Univ. of California.

Lipiec, J., and S. Tarkiewicz. 1990. "The influence of water content and bulk density on penetration resistance of two soils." *Zeszyty Problemowe Postępów Nauk Rolniczych* 388: 99–105.

Manfreda, S., L. Brocca, T. Moramarco, F. Melone, and J. Sheffield. 2014. "A physically based approach for the estimation of root-zone soil moisture from surface measurements." *Hydrol. Earth Syst. Sci.* 18 (3): 1199–1212. https://doi.org/10.5194/hess-18-1199-2014.

Mansell, R., L. Ma, L. Ahuja, and S. Bloom. 2002. "Adaptive grid refinement in numerical models for water flow and chemical transport in soil: A review." *Vadose Zone J.* 1 (2): 222–238. https://doi.org/10.2113/1.2.222.

Mohammad, N., A. Alazba, and J. Šimůnek. 2014. "HYDRUS simulations of the effects of dual-drip subsurface irrigation and a physical barrier on water movement and solute transport in soils." *Irrig. Sci.* 32 (2): 111–125. https://doi.org/10.1007/s00271-013-0417-x.

Naghedifar, S. M., A. N. Ziaei, and H. Ansari. 2018. "Simulation of irrigation return flow from a Triticale farm under sprinkler and furrow irrigation systems using experimental data: A case study in arid region." *Agric. Water Manage.* 210 (Nov): 185–197. https://doi.org/10.1016/j.agwat.2018.07.036.

Ochsner, E., M. H. Cosh, R. Cuenca, Y. Hagimoto, Y. Kerr, E. Njoku, and M. Zreda. 2013. "State of the art in large-scale soil moisture monitoring." *Soil Sci. Soc. Am. J.* 77 (6): 1888–1919. https://doi.org/10.2136/sssaj2013.03.0093.

Panday, S., and P. S. Huyakorn. 2008. "MODFLOW SURFACT: A state-of-the-art use of vadose zone flow and transport equations and numerical techniques for environmental evaluations." *Vadose Zone J.* 7 (2): 610–631. https://doi.org/10.2136/vzj2007.0052.

Puma, M. J., M. A. Celia, I. Rodriguez-Iturbe, and A. J. Guswa. 2005. "Functional relationship to describe temporal statistics of soil moisture averaged over different depths." *Adv. Water Resour.* 28 (6): 553–566. https://doi.org/10.1016/j.advwatres.2004.08.015.

Ragab, R. 1995. "Towards a continuous operational system to estimate the root-zone soil moisture from intermittent remotely sensed surface moisture." *J. Hydrol.* 173 (1–4): 1–25. https://doi.org/10.1016/0022-1694(95)02749-F.

Richards, F. 1959. "A flexible growth curve for empirical use." *J. Exp. Botany* 10 (2): 290–301. https://doi.org/10.1093/jxb/10.2.290.

Richards, L. A. 1931. "Capillary conduction of liquids through porous mediums." *Physics* 1 (5): 318–333. https://doi.org/10.1063/1.1745010.

Sabater, J. M., L. Jarlan, J.-C. Calvet, F. Bouyssel, and P. De Rosnay. 2007. "From near-surface to root-zone soil moisture using different assimilation techniques." *J. Hydrometeorol.* 8 (2): 194–206. https://doi.org/10.1175/JHM571.1.

Schaap, M. G., F. J. Leij, and M. T. van Genuchten. 2001. "Rosetta: A computer program for estimating soil hydraulic parameters with hierarchical pedotransfer functions." *J. Hydrol.* 251 (3–4): 163–176. https://doi.org/10.1016/S0022-1694(01)00466-8.

Simunek, J., M. T. van Genuchten, and M. Sejna. 2008. "Development and applications of the HYDRUS and STANMOD software packages and related codes." *Vadose Zone J.* 7 (2): 587–600. https://doi.org/10.2136/vzj2007.0077.

Simunek, J., M. T. Van Genuchten, and M. Sejna. 2005. *The HYDRUS-1D software package for simulating the one-dimensional movement of water, heat, and multiple solutes in variably-saturated media*. Univ. California-Riverside Research Rep. No. 3, 1–240. Oakland, CA: Univ. California-Riverside.

Šimůnek, J., and J. W. Hopmans. 2009. "Modeling compensated root water and nutrient uptake." *Ecol. Modell.* 220 (4): 505–521. https://doi.org/10.1016/j.ecolmodel.2008.11.004.

Spelman, D., K.-D. Kinzli, and T. Kunberger. 2013. "Calibration of the 10HS soil moisture sensor for southwest Florida agricultural soils." *J. Irrig. Drain. Eng.* 139 (12): 965–971. https://doi.org/10.1061/(ASCE)IR.1943-4774.0000647.

The MathWorks. n.d. "Genetic algorithm." Accessed July 30, 2025. https://www.mathworks.com/discovery/genetic-algorithm.html.

Tolk, J. A., and T. A. Howell. 2001. "Measured and simulated evapotranspiration of grain sorghum grown with full and limited irrigation in three high plains soils." *Trans. ASAE* 44 (6): 1553–1558. https://doi.org/10.13031/2013.7040.

van Dam, J. C., P. Groenendijk, R. F. Hendriks, and J. G. Kroes. 2008. "Advances of modeling water flow in variably saturated soils with SWAP." *Vadose Zone J.* 7 (2): 640–653. https://doi.org/10.2136/vzj2007.0060.

Van Genuchten, M. T. 1980. "A closed-form equation for predicting the hydraulic conductivity of unsaturated soils." *Soil Sci. Soc. Am. J.* 44 (5): 892–898. https://doi.org/10.2136/sssaj1980.03615995004400050002x.

Vázquez-Suñé, E., E. Abarca, J. Carrera, B. Capino, D. Gámez, M. Pool, T. Simó, F. Batlle, J. Niñerola, and X. Ibáñez. 2006. "Groundwater modelling as a tool for the European water framework directive (WFD) application: The Llobregat case." *Phys. Chem. Earth A/B/C* 31 (17): 1015–1029. https://doi.org/10.1016/j.pce.2006.07.008.

Vogel, M. 2019. *Effects of model spin-up on simulated recharge using the Hydrus-1D vadose zone model*. Uppsala, Sweden: Uppsala Univ.

Wagner, W., G. Lemoine, and H. Rott. 1999. "A method for estimating soil moisture from ERS scatterometer and soil data." *Remote Sens. Environ.* 70 (2): 191–207. https://doi.org/10.1016/S0034-4257(99)00036-X.

Wesseling, J., J. Elbers, P. Kabat, and B. Van den Broek. 1991. *SWATRE: Instructions for input*. Wageningen, Netherlands: Winand Staring Centre.

White, M. D., M. Oostrom, M. L. Rockhold, and M. Rosing. 2008. "Scalable modeling of carbon tetrachloride migration at the Hanford site using the STOMP simulator." *Vadose Zone J.* 7 (2): 654–666. https://doi.org/10.2136/vzj2007.0070.

Yang, T., J. Šimůnek, M. Mo, B. Mccullough-Sanden, H. Shahrokhnia, S. Cherchian, and L. Wu. 2019. "Assessing salinity leaching efficiency in three soils by the HYDRUS-1D and-2D simulations." *Soil Tillage Res.* 194 (Nov): 104342. https://doi.org/10.1016/j.still.2019.104342.

Zhang, H., R. Yang, S. Guo, and Q. Li. 2020. "Modeling fertilization impacts on nitrate leaching and groundwater contamination with HYDRUS-1D and MT3DMS." *Paddy Water Environ.* 18 (3): 481–498. https://doi.org/10.1007/s10333-020-00796-6.

Zhang, Y., W. Zhao, T. E. Ochsner, B. M. Wyatt, H. Liu, and Q. Yang. 2019. "Estimating deep drainage using deep soil moisture data under young irrigated cropland in a desert-oasis ecotone, Northwest China." *Vadose Zone J.* 18 (1): 1–10. https://doi.org/10.2136/vzj2018.10.0189.

Zhuang, R., Y. Zeng, S. Manfreda, and Z. Su. 2020. "Quantifying long-term land surface and root zone soil moisture over Tibetan Plateau." *Remote Sens.* 12 (3): 509. https://doi.org/10.3390/rs12030509.